

Electronic Supporting Information

The Excited-State Dynamics of the Radical Anions of Cyanoanthracenes

Joseph S. Beckwith,^a Alexander Aster,^b Eric Vauthey*

Department of Physical Chemistry, University of Geneva, 30 Quai Ernest-Ansermet, 1211 Genève 4, Switzerland

a Present address: Department of Chemistry, Princeton University, Princeton, New Jersey 08544, USA

b Present address: Solvias AG, Römerpark 2, 4303 Kaiseraugst, Switzerland

Contents

S1 Preparation of the radical anions	4
S2 Transient absorption setup	4
S3 Stationary absorption spectroscopy	5
S4 Quantum-Chemical Calculations	7
S5 Pump-Probe measurements	9
S6 Pump-Pump-Probe measurements	13
S7 Vibrational coherence	15

List of Figures

S1	Stationary absorption spectra of TrCA ⁻ in ACN solution. The areas taken for Band 1 and Band 2 are highlighted in red and blue respectively.	6
S2	Ratio of Band 1 and Band 2 (highlighted in Figure S1) across multiple measurements.	6
S3	Calculated transitions (gray sticks, CAM-B3LYP/aug. cc-pVDZ) plotted vs steady-state absorption spectra of a) DCA ⁻ , b) TrCA ⁻ , c) TCA ⁻ . Calculated transition energies are offset by -0.29 eV for DCA ⁻ , -0.2 eV for TrCA ⁻ , and -0.28 eV for TCA ⁻	7
S4	Transition densities associated with the lowest-energy absorption band (loss of electron density in blue, gain in red, CAM-B3LYP/aug. cc-pVDZ) of DCA ⁻ , TrCA ⁻ and TCA ⁻	7
S5	Energy-level diagrams obtained from TD-DFT calculations at the B3LYP/6-31+G* level.	8
S6	Evolution-associated difference absorption spectra and corresponding time constants obtained from a global analysis of the TA data measured with DCA , TrCA and TCA upon 400 nm excitation in ACN, assuming a series of two or three successive exponential steps.	9
S7	Evolution-associated difference absorption spectra and corresponding time constants obtained from a global analysis of the TA data measured with DCA ⁻ generated upon continuous irradiation of a DCA /TEA/TBADHP solution and negative stationary absorption spectrum of DCA	10
S8	Time dependence of the TA at different wavenumbers measured upon 710 nm excitation of DCA ⁻ generated upon continuous irradiation of a DCA /TEA/TBADHP solution. The concentration of TEA has no effect upon the excited-state dynamics even if changed by a factor of 4.	10
S9	Transient absorption spectra measured at different time delays after 400 nm excitation of DCA with 1 M TMB in ACN.	11
S10	Transient absorption spectra measured at different time delays after 400 nm excitation of DCA with 1 M TMB in DMF.	11
S11	Evolution-associated difference absorption spectra and corresponding time constants obtained from a global analysis of the TA data measured with TrCA ⁻ generated upon continuous irradiation of a TrCA /TEA/TBADHP solution and negative stationary absorption spectrum of DCA	11
S12	Transient absorption spectra measured at different time delays after 400 nm excitation of TrCA with 1 M MES in ACN.	12
S13	A) PPP spectra measured with DCA and 1 M TMB in DMF at different delays after the second pump pulse at 710 nm. The delay between the actinic pulse at 400 nm and the 710 nm pulse was 1 ns. B) Evolution-associated difference absorption spectra and time constants obtained from a global analysis of the PPP data assuming two successive exponential steps $A' \rightarrow B' \rightarrow C'$, C' being the D_0 state.	13
S14	A) PPP spectra measured with TrCA and 1 M MES in ACN at different delays after the second pump pulse at 710 nm. The delay between the actinic pulse at 400 nm and the 710 nm pulse was 1 ns. B) Evolution-associated difference absorption spectra and time constants obtained from a global analysis of the PPP data assuming two successive exponential steps $A' \rightarrow B' \rightarrow C'$, C' being the D_0 state.	14

S15	Contour plot of the residual obtained from a multiexponential global analysis of the transient absorption data measured upon 710 nm excitation of TrCA ⁻ generated upon continuous irradiation of a TrCA /TEA/TBADHP mixture in ACN.	15
S16	Fourier-transform spectrum of the transient absorption time profile at 16000 cm ⁻¹ . measured with TrCA ⁻ generated upon continuous irradiation of a TrCA /TEA/TBADHP mixture in ACN.	15
S17	Displacement vectors associated with the calculated 329 cm ⁻¹ vibrational mode of TrCA ⁻	16
S18	Contour plot of the residual obtained from a multiexponential global analysis of the transient absorption data measured upon 710 nm excitation of TrCA ⁻ generated upon continuous irradiation of a TCA /TEA/TBADHP mixture in ACN.	16
S19	Fourier-transform spectrum of the transient absorption time profile at 15000 cm ⁻¹ . measured with TCA ⁻ generated upon continuous irradiation of a TrCA /TEA/TBADHP mixture in ACN.	16
S20	Displacement vectors associated with the calculated 300 cm ⁻¹ vibrational mode of TCA ⁻	17

S1 Preparation of the radical anions

A ~ 3 mL solution of the chromophore ($\sim 2 \times 10^{-4}$ M), 0.22 M triethylamine and 5.4×10^{-3} M tetra-*n*-butylammonium dihydrogen phosphate in ACN was prepared and placed, along with two magnetic stirrer bars (one for stirring during the radical generation reaction and one for stirring during the ultrafast experiment)[1] in a sealable cuvette used for degassing via a Schlenk line. This solution was then degassed via the freeze-pump-thaw method at least 3 times, and kept sealed thereafter to remove the presence of oxygen as much as possible. This cuvette was then sealed and removed from the Schlenk line (to further seal the cuvette a stopper was placed in the connector to the Schlenk line and sealed with Parafilm), thawed and placed above a stirring plate. The solution was then continuously irradiated with an unfocussed 20 mW 405 nm diode laser (*Changchun New Industries Optoelectronics Technology, TEM₀₀ Mode Violet Blue Laser at 405 nm*) whilst being stirred for at least 1 hour, until a substantial yield of the radical anion was generated.

S2 Transient absorption setup

The setup for fs transient absorption used the output of an amplified Ti:sapphire system (Solstice Ace, *Spectra-Physics*), producing 35 fs pulses centred at 800 nm with a 5 kHz repetition rate. A fraction of the output of the amplifier was split into two for use as pump and probe. Before white-light generation, the probe beam was chopped to a frequency of 1 kHz (MC2000B Optical Chopper System with MC1F10A 10 Slot (20 % duty cycle) Chopper Blade, *Thorlabs*). White-light probe pulses were generated by focusing $\sim 1 \mu\text{J}$ of the fundamental in a 3 mm CaF₂ plate, detected with a pair of 163 mm spectrographs (SR163, *Andor Technology*) equipped with a 512×58 pixel back-thinned CCD (S07030-09, *Hamamatsu*) and assembled by Entwicklungsbüro Stresing, Berlin. The white-light beam was split into a signal and a reference path, for best signal-to-noise ratio.[2, 3, 4] One white-light probe beam was focussed to an approximately $60 \mu\text{m}$ diameter spot in the sample and overlapped with the pump beam, whereas the other was used as a reference. The probing range extended from about 320 to 750 nm, limited by the beamsplitter used to separate the residual fundamental and the white light and the grating in the spectrographs.

Pumping was achieved by using the output of a TOPAS-Prime in combination with a NirUVis module (*Light Conversion*), which produces pulses between $\sim 500 - 2000$ nm, with an output energy of $\sim 250 \mu\text{J}$ at the peak. These pulses were then compressed in a folded prism compressor made of SF10 glass (Schott) resulting in a pulse duration of 60 – 100 fs at the sample position. After generation, the pump pulse was reflected into a moveable delay stage (*Physik Instrumente*) to delay the pump pulse relative to the probe pulse by up to 2 ns. The step-scan method of collecting data was used.[5] The pump intensity on the sample was $\sim 0.15 - 0.75 \text{ mJ} \cdot \text{cm}^{-2}$. The pump was chopped to a frequency of 500 Hz (MC2000B Optical Chopper System with MC1F10A 10 Slot (10 % duty cycle) Chopper Blade, *Thorlabs*) such that 1 in 2 shots were pumped. The pump polarisation was set to magic angle with respect to that of the probe.

S3 Stationary absorption spectroscopy

Absorption spectra were recorded on a Cary 50 absorption spectrometer. Absorption spectra were baseline corrected by subtracting the spectra of the corresponding pure solvent. Absorption spectra were obtained using samples with a maximal absorbance of 1. For comparison with the TD-DFT calculations the oscillator strength of the lowest transition was calculated using:[6]

$$f = 4.39 \times 10^{-9} \left[\frac{1}{n} \frac{1}{f(n)} \times \int \varepsilon(\tilde{\nu}) d\tilde{\nu} \right] \quad (\text{S1})$$

where $\varepsilon(\tilde{\nu})$ is the molar absorption coefficient of the lowest energy transition and n is the refractive index of the solvent. In accordance with ref.7, $f(n)$, an effective cavity factor, was taken to be

$$f(n) = \frac{9n^2}{(2n^2 + 1)^2}. \quad (\text{S2})$$

The absorption transition dipole moment was calculated using[6]

$$\mu_{abs} = 9.584 \times 10^{-2} \left[\frac{1}{n} \frac{1}{f(n)} \times \int_{D_1 \text{band}} \frac{\varepsilon(\tilde{\nu})}{\tilde{\nu}} d\tilde{\nu} \right]^{1/2} \quad (\text{S3})$$

where $\varepsilon(\tilde{\nu})$ is the molar absorption coefficient of the $D_1 \leftarrow D_0$ transition and n is the refractive index of the solvent.

Absorption band of $\text{TrCA}^{\cdot-}$ at $12,000 \text{ cm}^{-1}$

To determine if the weak band at $12,000 \text{ cm}^{-1}$ was a scattering artefact or a genuine absorption of the $\text{TrCA}^{\cdot-}$ chromophore, multiple preparations (5 in total) and multiple absorption experiments on each of these were done. If the band at $12,000 \text{ cm}^{-1}$ were from the $\text{TrCA}^{\cdot-}$ anion, it should be present in the same ratio to the band at $14,000 \text{ cm}^{-1}$ in all of these experiments. Figure S2 shows that ratio of the band area around these two wavenumbers (Figure S1) varies across multiple experiments. Based on this, this feature is not assigned as arising from $\text{TrCA}^{\cdot-}$.

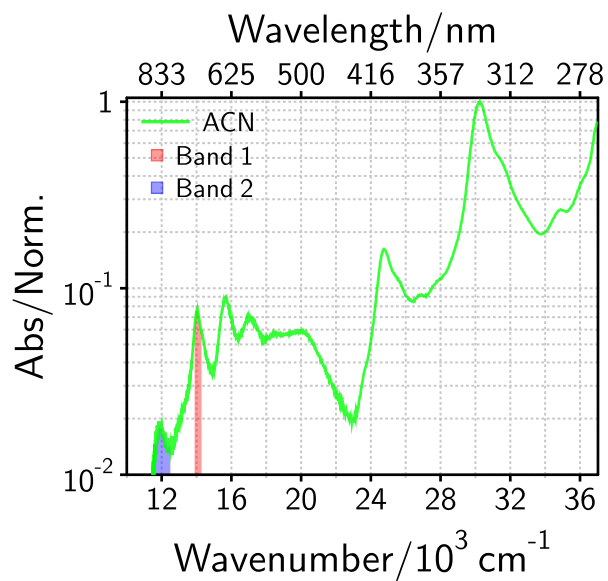


Figure S1: Stationary absorption spectra of TrCA^- in ACN solution. The areas taken for Band 1 and Band 2 are highlighted in red and blue respectively.

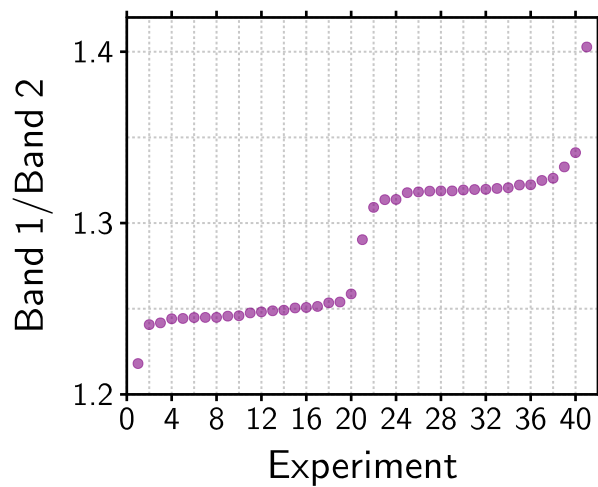


Figure S2: Ratio of Band 1 and Band 2 (highlighted in Figure S1) across multiple measurements.

S4 Quantum-Chemical Calculations

TD-DFT was used to calculate the excitation energies and the corresponding oscillator strengths of the three radical anions. The predicted transition energies obtained at the CAM-B3LYP/aug. cc-pVDZ level are plotted in Figure S3 vs the experimental absorption spectra.

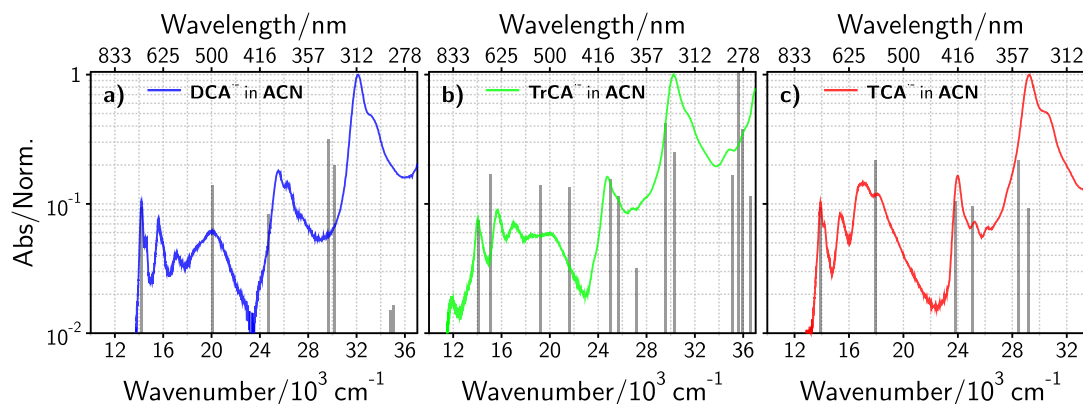


Figure S3: Calculated transitions (gray sticks, CAM-B3LYP/aug. cc-pVDZ) plotted vs steady-state absorption spectra of **a) DCA^{•-}**, **b) TrCA^{•-}**, **c) TCA^{•-}**. Calculated transition energies are offset by -0.29 eV for **DCA^{•-}**, -0.2 eV for **TrCA^{•-}**, and -0.28 eV for **TCA^{•-}**.

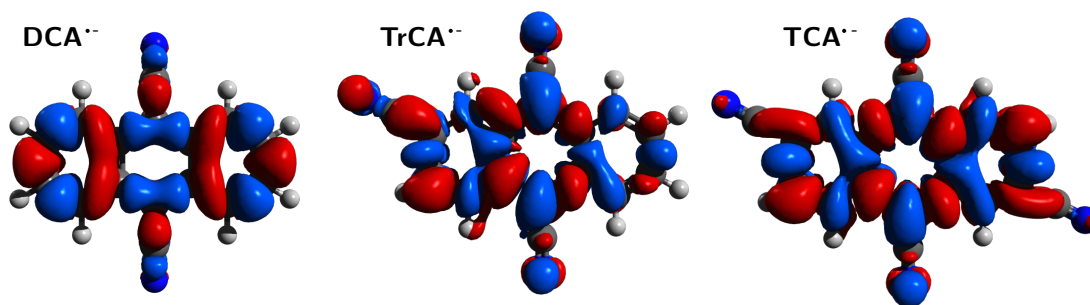


Figure S4: Transition densities associated with the lowest-energy absorption band (loss of electron density in blue, gain in red, CAM-B3LYP/aug. cc-pVDZ) of **DCA^{•-}**, **TrCA^{•-}** and **TCA^{•-}**.

Agreement (after shifting of the lowest energy band by 0.2-0.3 eV) is reasonable. In the following discussion, the reader is reminded that here the SOMO refers to the singly occupied molecular orbital and the LUMO to be the lowest *completely* unoccupied molecular orbital. For **DCA^{•-}**, the lowest energy absorption band is predicted to be dominated by a one electron transition from the SOMO-1 to the SOMO.

For **TrCA^{•-}**, this is predicted to be associated with both a transition from the SOMO to the LUMO+1 (59%) and a transition from the SOMO-1 to the SOMO (30%).

Finally, for **TCA^{•-}**, the first allowed transition is due mostly to a transition from the SOMO-1 to the SOMO. These transitions are shown in Figure S4.

Figure S5 shows the results from TD-DFT calculations at the B3LYP/6-31+G* level performed at the D_0 equilibrium geometry as well as at the D_1 and D_2 equilibrium geometries for $\text{DCA}^{\cdot-}$ and $\text{TCA}^{\cdot-}$. The results at the D_0 geometry are qualitatively the same as those obtained with CAM-B3LYP/aug. cc-pVDZ.

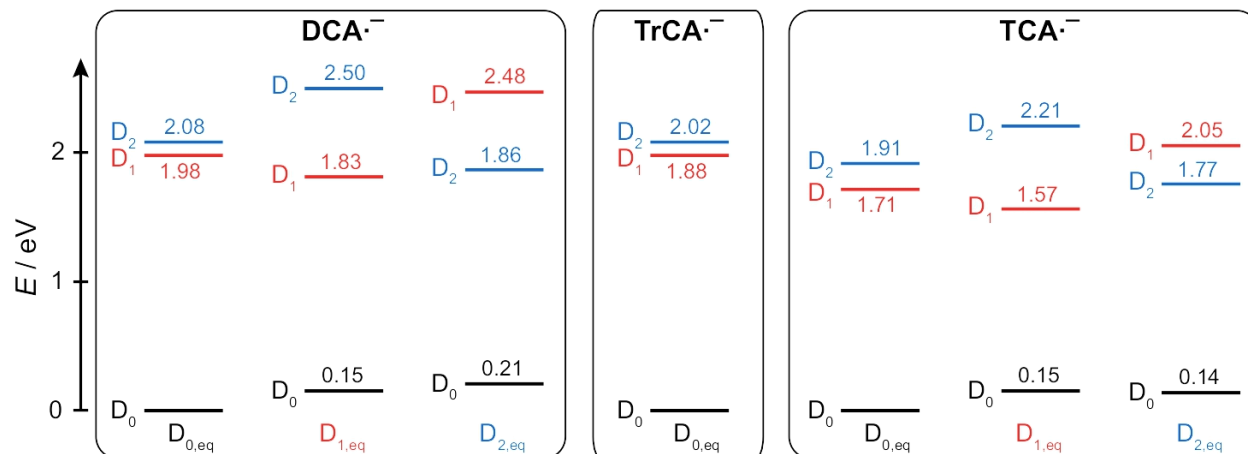


Figure S5: Energy-level diagrams obtained from TD-DFT calculations at the B3LYP/6-31+G* level.

S5 Pump-Probe measurements

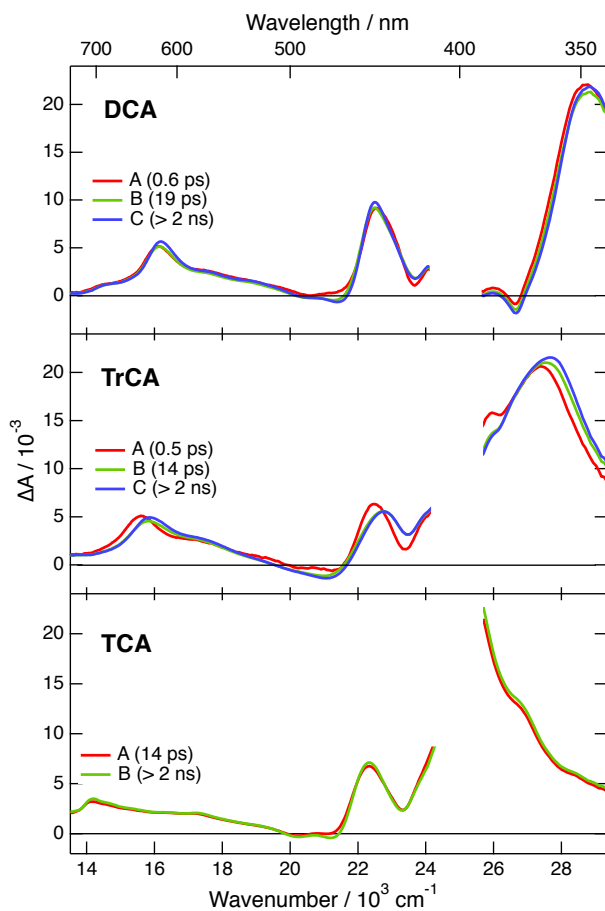


Figure S6: Evolution-associated difference absorption spectra and corresponding time constants obtained from a global analysis of the TA data measured with **DCA**, **TrCA** and **TCA** upon 400 nm excitation in ACN, assuming a series of two or three successive exponential steps.

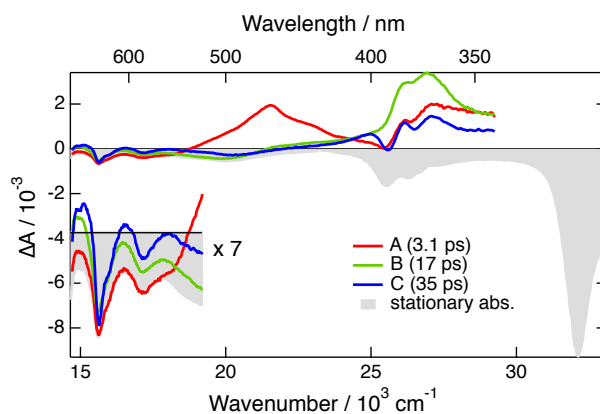


Figure S7: Evolution-associated difference absorption spectra and corresponding time constants obtained from a global analysis of the TA data measured with $\text{DCA}^{\cdot-}$ generated upon continuous irradiation of a $\text{DCA}/\text{TEA}/\text{TBADHP}$ solution and negative stationary absorption spectrum of DCA .

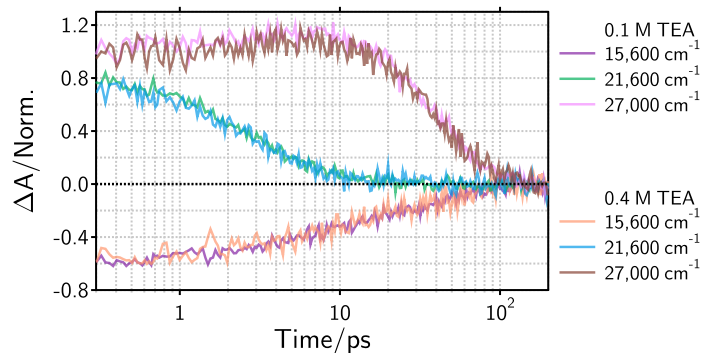


Figure S8: Time dependence of the TA at different wavenumbers measured upon 710 nm excitation of $\text{DCA}^{\cdot-}$ generated upon continuous irradiation of a $\text{DCA}/\text{TEA}/\text{TBADHP}$ solution. The concentration of TEA has no effect upon the excited-state dynamics even if changed by a factor of 4.

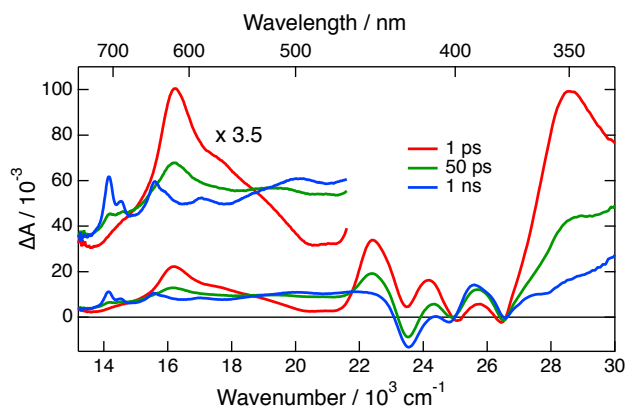


Figure S9: Transient absorption spectra measured at different time delays after 400 nm excitation of **DCA** with 1 M TMB in ACN.

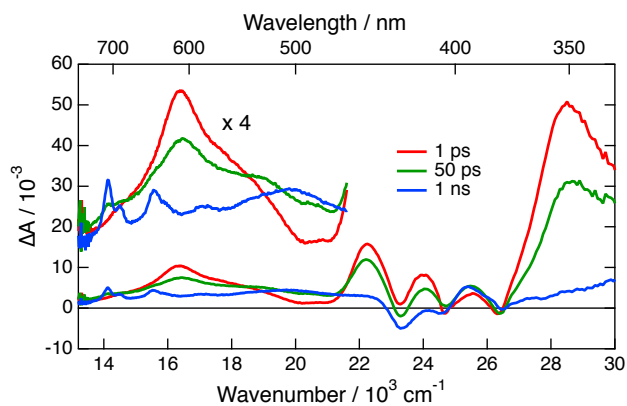


Figure S10: Transient absorption spectra measured at different time delays after 400 nm excitation of **DCA** with 1 M TMB in DMF.

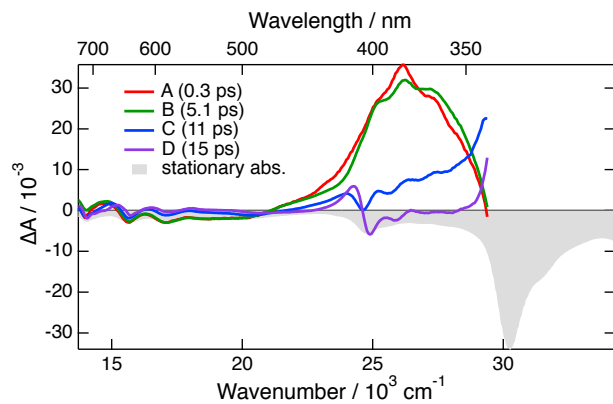


Figure S11: Evolution-associated difference absorption spectra and corresponding time constants obtained from a global analysis of the TA data measured with **TrCA**^{·-} generated upon continuous irradiation of a **TrCA**/TEA/TBADHP solution and negative stationary absorption spectrum of **DCA**.

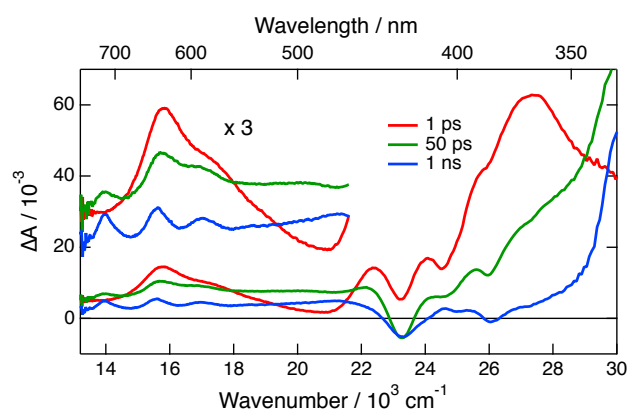


Figure S12: Transient absorption spectra measured at different time delays after 400 nm excitation of **TrCA** with 1 M MES in ACN.

S6 Pump-Pump-Probe measurements

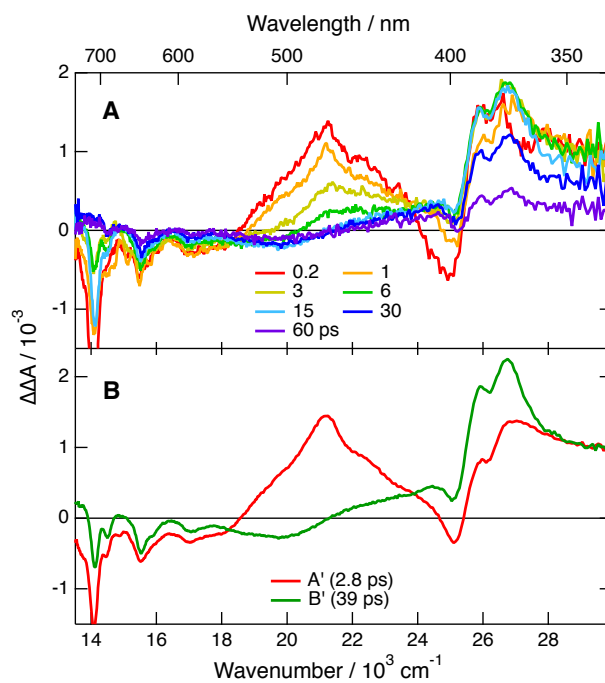


Figure S13: A) PPP spectra measured with **DCA** and 1 M TMB in DMF at different delays after the second pump pulse at 710 nm. The delay between the actinic pulse at 400 nm and the 710 nm pulse was 1 ns. B) Evolution-associated difference absorption spectra and time constants obtained from a global analysis of the PPP data assuming two successive exponential steps $A' \rightarrow B' \rightarrow C'$, C' being the D_0 state.

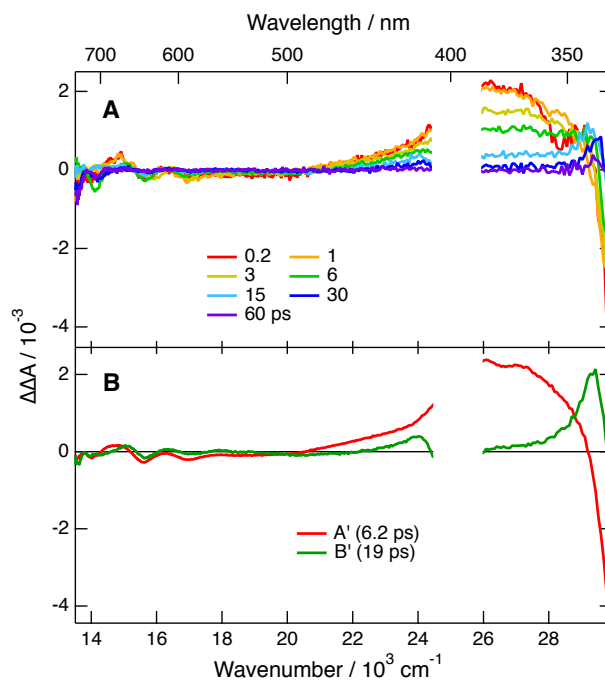


Figure S14: A) PPP spectra measured with **TrCA** and 1 M MES in ACN at different delays after the second pump pulse at 710 nm. The delay between the actinic pulse at 400 nm and the 710 nm pulse was 1 ns. B) Evolution-associated difference absorption spectra and time constants obtained from a global analysis of the PPP data assuming two successive exponential steps $A' \rightarrow B' \rightarrow C'$, C' being the D_0 state.

S7 Vibrational coherence

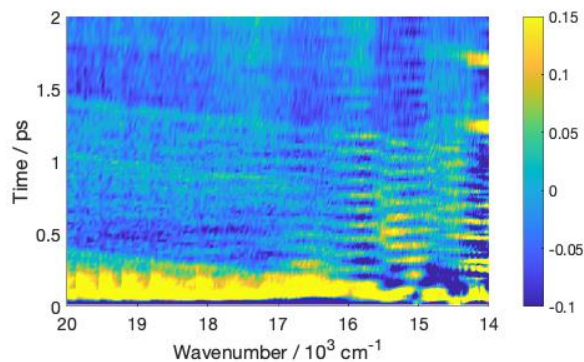


Figure S15: Contour plot of the residual obtained from a multiexponential global analysis of the transient absorption data measured upon 710 nm excitation of **TrCA**⁻ generated upon continuous irradiation of a **TrCA**/TEA/TBADHP mixture in ACN.

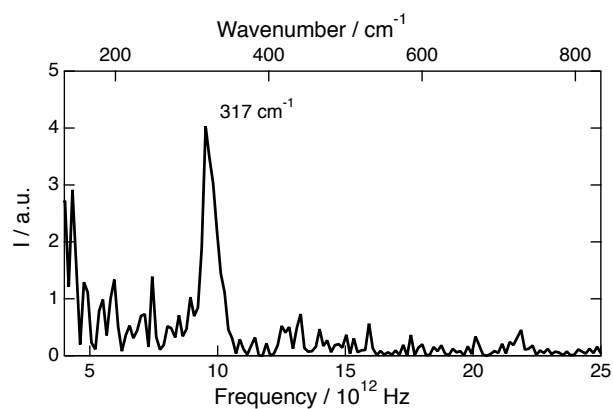


Figure S16: Fourier-transform spectrum of the transient absorption time profile at 16000 cm⁻¹, measured with **TrCA**⁻ generated upon continuous irradiation of a **TrCA**/TEA/TBADHP mixture in ACN.

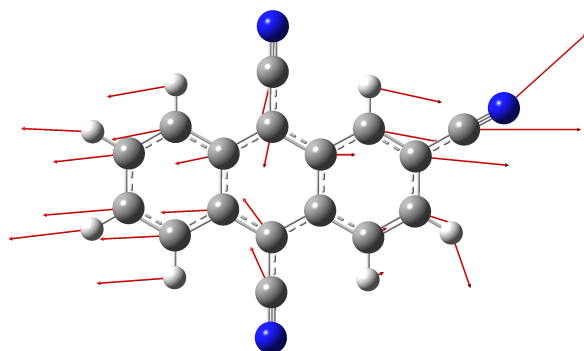


Figure S17: Displacement vectors associated with the calculated 329 cm^{-1} vibrational mode of TrCA^- .

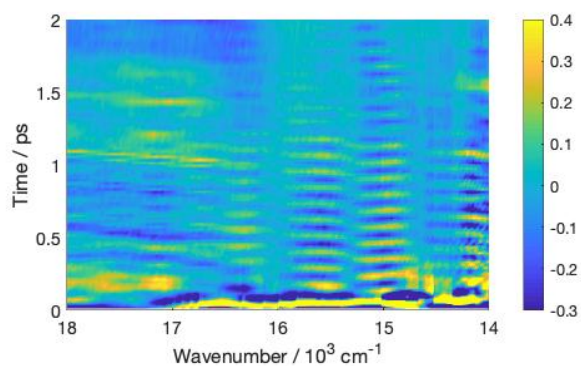


Figure S18: Contour plot of the residual obtained from a multiexponential global analysis of the transient absorption data measured upon 710 nm excitation of TrCA^- generated upon continuous irradiation of a $\text{TCA}/\text{TEA}/\text{TBADHP}$ mixture in ACN .

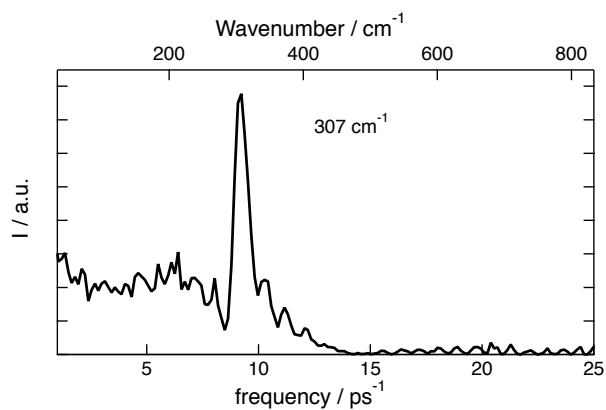


Figure S19: Fourier-transform spectrum of the transient absorption time profile at 15000 cm^{-1} , measured with TCA^- generated upon continuous irradiation of a $\text{TrCA}/\text{TEA}/\text{TBADHP}$ mixture in ACN .

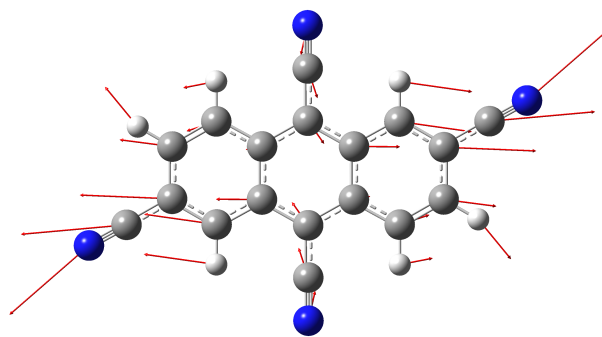


Figure S20: Displacement vectors associated with the calculated 300 cm^{-1} vibrational mode of TCA^- .

References

- [1] P. N. Dominguez, F. T. Lehner, J. Michelmann, M. Himmelstoss and W. Zinth, *Rev. Sci. Instrum.*, 2015, **86**, 033101.
- [2] A. L. Dobryakov, S. A. Kovalenko, A. Weigel, J. L. Pérez-Lustres, J. Lange, A. Müller and N. P. Ernsting, *Rev. Sci. Instrum.*, 2010, **81**, 113106.
- [3] M. Bradler and E. Riedle, *J. Opt. Soc. Am. B*, 2014, **31**, 1465–1475.
- [4] B. Lang, *Rev. Sci. Instrum.*, 2018, **89**, 093112.
- [5] M. J. Feldstein, P. Vöhringer and N. F. Scherer, *J. Opt. Soc. Am. B*, 1995, **12**, 1500–1510.
- [6] J. B. Birks, *Photophysics of Aromatic Molecules*, Wiley-Interscience, London, New York, 1970.
- [7] D. Toptygin, *J. Fluoresc.*, 2003, **13**, 201–219.